

Robust lattice manipulation beyond nearest-neighbor coupling by pulsed electric fieldShuang Xu ¹, Wei-Jiang Gong,¹ H. Z. Shen,^{2,3} and X. X. Yi^{2,3,*}¹*College of Sciences, Northeastern University, Shenyang 110819, China*²*Center for Quantum Sciences and School of Physics, Northeast Normal University, Changchun 130024, China*³*Center for Advanced Optoelectronic Functional Materials Research, and Key Laboratory for UV Light-Emitting Materials and Technology of Ministry of Education, Northeast Normal University, Changchun 130024, China* (Received 29 August 2021; revised 14 November 2021; accepted 4 January 2022; published 13 January 2022)

In this paper, we propose an approach to manipulate a translation-invariant single-band tight-binding system beyond nearest-neighbor coupling. By using a sequence of multiple identical pulsed electric fields with specific strengths and calculated intervals, the propagator of the system can be fully controlled within an infinite space with dimensions given by the configuration of existing nonzero couplings. And if the sequence is repeated, the system evolution can then effectively simulate another system with a different array of hopping energies, provided that these hopping energies are already nonzero in the simulator. Moreover, the effective system's response to a wide range of additional influences, which are not required to be small, is also shown to approach that of the system it simulates in the limit of high kicking frequency. The simulation is therefore robust and the simulator can potentially be indistinguishable from the lattice it simulates. Considering the physical simplicity, this approach cannot only realize flexible experimental platforms for lattices beyond nearest-neighbor coupling, it is also potentially applicable to the manipulation of actual materials.

DOI: [10.1103/PhysRevB.105.014307](https://doi.org/10.1103/PhysRevB.105.014307)**I. INTRODUCTION**

Dynamics in translational-invariant lattices has long been under intense scrutiny. For one-dimensional (1D) single-band lattices with periodical boundary conditions, i.e., quantum rings characterized by tight-binding models, there has been intense research into the effect of controlled magnetic flux [1–3]. Through gauge transformation, the same model can be generalized to characterize lattices subject to a homogeneous electric field, for which the influence of pulsed [4–7], static [8–10], and alternating [2,11–17] electric fields have also been extensively examined. As experimental technologies advance, many interesting long predicted phenomena can finally be observed, such as Bloch oscillation [8,9,18], Aharonov-Bohm oscillations [19,20], persistent current [21–25], negative motion [26–31], speed limit [17,32,33], and dynamical localization [4–6,11–15].

However, most of the research is within the regime of nearest-neighbor coupling, while the effect of long-range hopping [10,34–36] has been shown as nontrivial and potentially relevant [37–39]. Experimental platforms with hopping coefficients beyond the nearest-neighbor coupling have been found [40–42], but realizing a high degree of flexibility in the coupling coefficients remains a challenge. Recently, based on cold atom simulation of tight-binding models, a helix lattice system was proposed [43], in which long-range couplings are somewhat controllable through the shape of the lattice. Also, manipulation of up to two hopping coefficients was shown using static electric field [10].

In this paper, we propose an approach using sequences of pulsed electric field to realize a flexible Floquet engineering [44–49] that controls all existing nonzero hopping coefficients in a single-band lattice with long-range hopping. The formalism for this approach begins in the model of 1D single-band tight-binding rings pierced by magnetic flux. Using the commutation relations among the different hopping components in the system Hamiltonian, we decompose the dynamics of the system and map the propagator of the lattice as a collection of moving points within two-dimensional (2D) real space. With few given exceptions notwithstanding, we prove that the array of coordinates of these points has one-to-one correspondence with the propagator. Moreover, we find the movements of these points governed by simple principles: each of them moves at a fixed speed determined by the corresponding hopping energy, and the magnetic flux determines each of the motion directions.

Subsequently, by considering the limit of large site number, we ignore the periodical boundary condition, which equates the tight-binding ring with a lattice and replaces the magnetic flux with a homogeneous electric field. Under a series of kicks by pulsed electric field with a specific strength and controllable time intervals [7], we show how the displacement of these moving points can be explicitly and independently controlled. Therefore, an arbitrary propagator that exists on the map can therefore be realized, which can be chosen as identical to the short-time propagator of a different lattice with the same configuration of nonzero couplings. The same propagator can then be applied repeatedly using the same sequence of pulsed electric field at a high frequency, turning a lattice into a flexible Floquet simulator of lattices with an explicitly chosen array of hopping parameters.

*yixx@nenu.edu.cn

Furthermore, in the limit of high kicking frequency, it can be shown that the simulator lattice will not only faithfully observe the same evolution, but also respond to external influences in the same way as the indented effective system. Such external influences may include arbitrary interactions with an environment, as well as defects, electron-electron interactions, and certain band-band interactions. Therefore, if one were to overcome limitations on the kicking frequency such as the effect of heating, it is ideally possible for the simulator lattice to be indistinguishable from the lattice it simulates to an observer unaware of the pulsed electric field.

The remaining of this paper is arranged as follows. In Sec. II, we establish the one-to-one correspondence between the propagator of a single-band tight-binding ring or lattice and the coordinates of a set of moving points in 2D real space. We also examine the dynamics of these points and show how the formalism can be generalized to lattices of higher dimensions. In Sec. III, we present an approach based on a sequence of pulsed electric field that controls the propagator of a single-band lattice with arbitrary long-range hopping, which allows the lattice to simulate different lattice parameters. In Sec. IV, we show that, in the limit of high kicking frequency, the simulation is robust against arbitrary external influences. Finally, in Sec. V, we summarize our results.

II. FORMALISM

We begin by generally characterizing a 1D single-band N -site translation-invariant tight-binding ring, which is also assumed as pierced by a time-dependent magnetic flux and containing up to the M th nearest-neighbor coupling. Ignoring electron-electron interactions, the Hamiltonian of the system reads

$$H(t) = \sum_{m=1}^M H_m(\phi_t), \quad (1)$$

$$H_m(\phi_t) \equiv J_m[\epsilon_{-m}(\phi_t) + \epsilon_{+m}(\phi_t)], \quad (2)$$

$$\epsilon_m(\phi_t) \equiv \sum_{j=1}^N e^{-im\frac{\phi_t}{N}} c_{j+m}^\dagger c_j, \quad (3)$$

where c_j is the fermionic annihilation operator of the j th lattice site, J_m is the hopping energy between the m th nearest neighbor, and ϕ_t is the magnetic flux through the ring at time t . Also, units of $\hbar = e = 1$ are used, and the periodical boundary condition of the ring dictates that indices j of c_j are always modulo N .

A. Map of propagator

To decompose the propagator of the system, we take advantage of the commutation relations of fermionic operators c_j , which conveniently give

$$[\epsilon_m(\phi), \epsilon_n(\phi')] = 0, \quad (4)$$

where m, n are arbitrary integers and ϕ, ϕ' are arbitrary magnetic flux. In particular, $[H_m(\phi), H_{m'}(\phi')] = 0$ makes it possible to write the propagator as a product of several

independent components:

$$U(t, t_0) \equiv e^{-i\int_{t_0}^t H(\tau)d\tau} = \prod_{m=1}^M e^{-i\int_{t_0}^t H_m(\tau)d\tau}. \quad (5)$$

To further simplify each of the components, we Fourier transform modes c_j into Bloch modes b_k using

$$b_k = \frac{1}{\sqrt{N}} \sum_j e^{-2\pi i \frac{jk}{N}} c_j, \quad (6)$$

$$c_j = \frac{1}{\sqrt{N}} \sum_k e^{2\pi i \frac{jk}{N}} b_k, \quad (7)$$

where k denotes Bloch momentum. Then, considering that $(b_k^\dagger b_k)^2 = b_k^\dagger b_k$, Eq. (2) gives

$$e^{-i\int_{t_0}^t H_m(\tau)d\tau} = \sum_k e^{-i\varphi_{mk}(t, t_0)} b_k^\dagger b_k, \quad (8)$$

$$\begin{aligned} \varphi_{mk}(t, t_0) &\equiv 2J_m \int_{t_0}^t \cos \left[m \left(\frac{\phi_\tau}{N} + 2\pi \frac{k}{N} \right) \right] d\tau, \\ &= 2\pi [\vec{r}_{mk} \cdot \vec{R}_m(t, t_0)], \end{aligned} \quad (9)$$

$$\vec{r}_{mk} \equiv \begin{bmatrix} \cos \frac{2\pi mk}{N} \\ \sin \frac{2\pi mk}{N} \end{bmatrix}, \quad (10)$$

$$\vec{R}_m(t, t_0) \equiv \int_{t_0}^t \frac{J_m}{\pi} \begin{bmatrix} \cos \frac{m\phi_\tau}{N} \\ -\sin \frac{m\phi_\tau}{N} \end{bmatrix} d\tau, \quad (11)$$

where $\varphi_{mk}(t, t_0)$ characterizes the phase-shift contribution from the m th nearest-neighbor coupling of an electron on fermionic mode b_k during the period between t_0 and t . Furthermore, since the dependency of $\varphi_{mk}(t, t_0)$ on ϕ_t and indices k are separated into an inner product of two vectors in a real 2D plane, the propagator of the system can thereby be reduced to

$$U(t, t_0) = \prod_m \mathcal{U}_m[\vec{R}_m(t, t_0)], \quad (12)$$

$$\mathcal{U}_m[\vec{R}_m(t, t_0)] \equiv \sum_k e^{-i\{2\pi[\vec{r}_{mk} \cdot \vec{R}_m(t, t_0)]\}} b_k^\dagger b_k. \quad (13)$$

The evolution of electrons on the lattice is thereby mapped to the movement of several vectors in a real 2D plane. Note that the function \mathcal{U}_m itself is given by the number of sites N alone, while vector $\vec{R}_m(t, t_0)$ only accounts for the influence of hopping energy and magnetic flux.

Moreover, given the integrand in Eq. (11), the nature of vector $\vec{R}_m(t, t_0)$ is easy to characterize. If one imagine the evolution of each vector $\vec{R}_m(t, t_0)$ as the coordinate of a point in the 2D plane, then each of them moves at a fixed speed $\frac{J_m}{\pi}$ that is only determined by the corresponding hopping energy. On the other hand, the magnetic flux only controls the direction of its movement.

B. Generalization and analysis

Although the map of propagator given by Eqs. (10)–(13) is established for tight-binding quantum rings threaded with magnetic flux, the same model, and hence the map, is also applicable to a 1D lattice in a time-dependent

homogeneous electric field. To obtain the specific correspondence, we consider a gauge transformation with unitary $G(t) \equiv \sum_j \exp(ij\frac{\phi_t}{N})c_j^\dagger c_j$, and the system Hamiltonian from Eq. (1) is transformed into

$$\mathcal{H} = G(t)H(t)G^{-1}(t) + i\frac{\partial G(t)}{\partial t}G^{-1}(t) = \mathcal{H}_b + \mathcal{H}_e, \quad (14)$$

$$\mathcal{H}_b = \sum_{m=1}^M J_m \sum_{j=1}^{N-m} [c_{j-m}^\dagger c_j + c_{j+m}^\dagger c_j] - \frac{\partial \phi_t}{N \partial t} \sum_j j c_j^\dagger c_j, \quad (15)$$

$$\mathcal{H}_e = \sum_{m=1}^M J_m \left[\sum_{j=0}^{m-1} e^{i\phi_t} c_j^\dagger c_{N-m+j} + \sum_{j=1}^{m-1} e^{-i\phi_t} c_{N-m+j}^\dagger c_j \right], \quad (16)$$

where \mathcal{H}_b is apparently the same formalism as the bulk of a 1D lattice subject to an electric field characterized by scalar potential. Note that \mathcal{H}_b no longer satisfies permutation symmetry. Compared with $H(t)$, the removal of these extra terms in \mathcal{H}_e leads to a discontinuity between mode c_0 and c_{N-1} in \mathcal{H}_b . Nevertheless, in the limit of $N \rightarrow \infty$, $M \ll N$, and if none of the electrons goes near the two ends of the lattice, \mathcal{H}_e can be ignored, i.e., $\mathcal{H} \rightarrow \mathcal{H}_b$. The dynamics of the electrons is then fully characterized by \mathcal{H}_b . In this case, we note that the last term on the right-hand side of Eq. (15) is in the form of a scalar potential. The correspondence between a magnetic flux ϕ_t and a time-dependent homogeneous electric field E_t is thereby characterized by

$$-\frac{\partial \phi_t}{N \partial t} = aE_t, \quad (17)$$

where a is the lattice constant, i.e., the distance between two nearest-neighboring sites. Moreover, we note that the same formalism thus far can also be applied to lattices of higher dimensions within the single-band regime. Apparently, the formalism Eq. (1) would hold under substitution $m \rightarrow \vec{m}$, $j \rightarrow \vec{j}$, and $m\frac{\phi_t}{N} \rightarrow \vec{l}(\vec{m}) \cdot \vec{A}(t)$, where integer vector \vec{m} characterizes the hopping distance in each direction in unit of site indices, $\vec{l}(\vec{m})$ denotes the corresponding physical displacement, and $\vec{A}(t)$ is a homogenous magnetic vector potential.

Another interesting aspect to this map of propagators is its periodicity or lack thereof. In a quantum ring of $N = 6$, for example, the function \mathcal{U}_1 is periodical. As shown in Fig. 1(a), one can find an example of a nonzero \vec{R}_1 so $\mathcal{U}_1(\vec{R}_1) = I$. And Fig. 1(b) shows clearly that there are many \vec{R}_1 on the 2D plane that lead to a return to the initial state. However, the case of $N = 6$ is more of an exception than the rule. In general, we obviously have

$$\forall \vec{\alpha}, \vec{\beta} \in \mathbb{R}^2 : \mathcal{U}_m(\vec{\alpha} + \vec{\beta}) = \mathcal{U}_m(\vec{\alpha})\mathcal{U}_m(\vec{\beta}), \quad (18)$$

and it can be shown that $\exists \vec{R}_1 \neq 0, w \in \mathbb{R} : \mathcal{U}_1(\vec{R}_1) = Ie^{-iw}$, if and only if $N = 2, 3, 4, 6$ (see Appendix A). In other words, for a 1D translation-invariant tight-binding ring with five or more than six sites and nearest-neighbor coupling, locations on the 2D map correspond one-to-one with all possible propagators within the control of magnetic flux. Moreover, in the limit of $N \rightarrow \infty$, it can be shown that $U(t, t_0) = Ie^{-iw}$ if and only if $\forall m : \vec{R}_m(t, t_0) = 0$ (see Appendix B). It thereby follows that the propagator $U(t, t_0)$ of a single-band translational-invariant lattice has one-to-one correspondence with the array of vectors $\vec{R}_m(t, t_0)$. It also follows that a wave

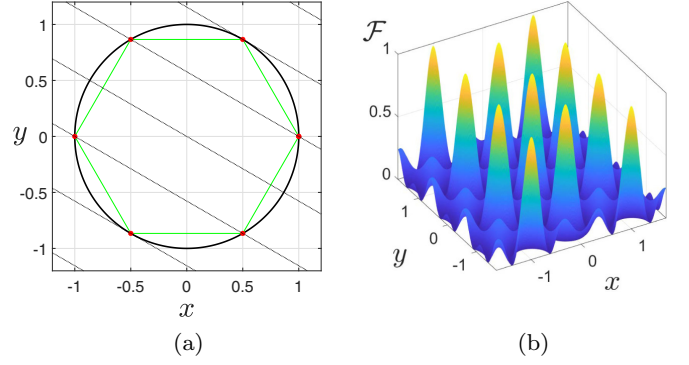


FIG. 1. Illustrations of the xy plane that \vec{R}_1 and \vec{r}_{1k} reside for a tight-binding ring of $N = 6$. (a) The black circle is the unit circle, on which the red dots are \vec{r}_{1k} , $k = 0, \dots, 5$, which in turn are the vertices of a green regular hexagon. The black dotted lines are the contour lines of integer values of function $f(\vec{r}) = \vec{r} \cdot \vec{R}_1$, with $\vec{R}_1 = [1 \quad \sqrt{3}]^T$. Note that for all k , $f(\vec{r}_{1k}) \in \mathbb{Z}$, which entails that phase shifts $\varphi_{1k}(t, t_0)$, as given in Eq. (9), are all integer multiples of 2π . (b) The self-fidelity of a single-site initial state $\mathcal{F}(\vec{R}_1) = |\langle \text{vac} | c_n \mathcal{U}_1(\vec{R}_1) c_n^\dagger | \text{vac} \rangle|^2$.

packet of arbitrary shape propagating in a lattice cannot be guaranteed to recover its shape at a different location, since guaranteeing $U(t, 0)\psi_0 = \epsilon_m(0)\psi_0 e^{-iw}$ for arbitrary initial wave function ψ_0 would require $U(t, 0) = \epsilon_m(0)e^{-iw}$, which would in turn entail $U(nt, 0) = [U(t, 0)]^n = Ie^{-inw}$.

III. MANIPULATION

In the following, we focus on a 1D lattice subject to homogeneous pulsed electric field similar to those examined by Ravindranath and Santhanam [7] for lattices beyond nearest-neighbor coupling. Using the map of propagator as points on a 2D space, we will show how a sequence of identical electric pulses can be engineered to navigate these moving points to arbitrary destinations independently. This in turn enables us to manipulate the lattice propagator during the whole sequence, which can then also be repeated so the lattice under the influence would undergo the evolution of a different lattice.

A. Navigation of the propagator

According to Eq. (17), the presence of an electric field is physically equivalent to altering magnetic flux; we can then effectively shift the magnetic flux with pulsed electric field, which will turn the direction of $\frac{\partial}{\partial t} \vec{R}_m$ and enable the navigation of \vec{R}_m . The impact of an electric pulse during a period of time Δt reads

$$K \equiv a \int_{t_0}^{t_0 + \Delta t} E_\tau d\tau = \frac{\phi_{t_0 + \Delta t}}{N} - \frac{\phi_{t_0}}{N}. \quad (19)$$

Apparently, in the scenario where Δt is very small, i.e., a kick, a sudden shift in ϕ_t will occur. This shift is directly given by K , which is therefore the strength of the kick. We then focus on an ideal sequence of identical pulsed electric field consisting of L kicks, each with the specific strength

$$K = \frac{2\pi}{L}. \quad (20)$$

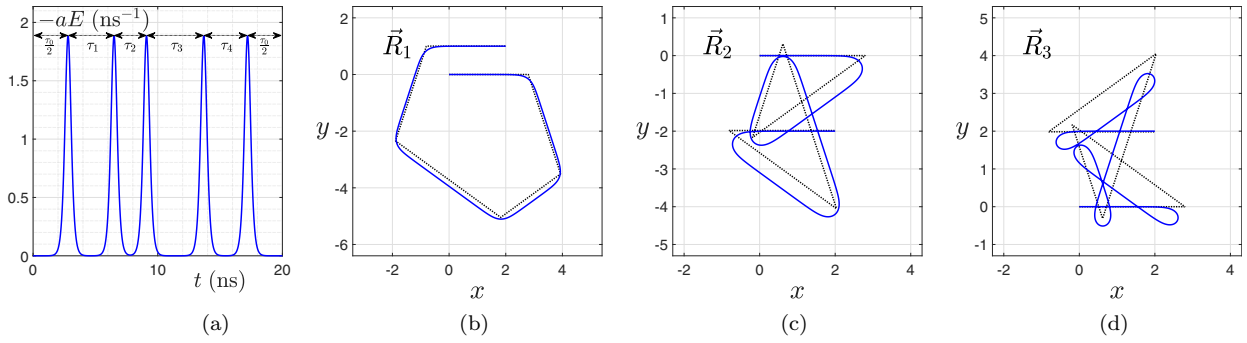


FIG. 2. Demonstration of navigating \vec{R}_m with electric field pulses of $L = 5$. (a) The pulsed electric field employed. These pulses can be characterized by $\frac{\phi_i}{N} = \frac{\pi}{L} \sum_{j=0}^{L-1} [\tanh \frac{t-t_j}{\Delta t} + 1]$ and Eq. (17), with $\Delta t = 3$ ns controlling the shape of the pulse. The intervals between pulse time t_j are given by $\mathbf{Q} = [20, 2+i, 2-2i, 2+2i, 2-i]$ ns and Eq. (25). For simplicity, the evolution begins at the middle of interval τ_0 . In (b)–(d), the blue solid curves are trajectories of $\vec{R}_m(t, 0)$ under the pulses shown in (a). Each of them begins at the point of origin and moves according to Eq. (11) with $J_m \equiv \pi$ ns $^{-1}$. In comparison, the black dotted lines are trajectories of $\vec{R}_m(t, 0)$ under ideally sharp pulses with $\Delta t \rightarrow 0$. In this case, the pulses are characterized by $\frac{\phi_i}{N} = \frac{2\pi}{L} \sum_{j=0}^{L-1} \Theta(t - t_j)$, where $\Theta(t)$ denotes Heaviside step function.

Recall that the velocity of each moving \vec{R}_m is simply the integrand in Eq. (11). Each shift in ϕ_i as characterized by Eq. (19) only changes their moving directions, while the intervals between these shifts are denoted by τ_l . The total displacement of vector \vec{R}_m at the end of the whole sequence then simply reads

$$\vec{R}_m = \frac{J_m}{\pi} \sum_{l=0}^{L-1} \tau_l \begin{bmatrix} \cos \frac{2\pi ml}{L} \\ -\sin \frac{2\pi ml}{L} \end{bmatrix}. \quad (21)$$

Apparently, the displacement of each \vec{R}_m at the end of the sequence is controlled by the array of time intervals $\boldsymbol{\tau} \equiv \{\tau_l\}$. Also, the special strength given in Eq. (20) makes the relation particularly convenient, since the equation above can be rewritten as

$$\mathbf{Q} \equiv \{Q_m\} = \mathcal{F}\boldsymbol{\tau}, \quad (22)$$

$$\frac{J_m}{\pi} Q_m = \vec{R}_m \cdot (\hat{x} + i\hat{y}), \quad (23)$$

$$Q_0 \equiv \sum_{l=0}^{L-1} \tau_l, \quad (24)$$

where \mathcal{F} is simply the discrete Fourier transformation and the contribution of J_m is introduced separately. The intervals required to realize an arbitrary \vec{R} are then explicitly solvable by combining Eq. (23) with

$$\boldsymbol{\tau} = \mathcal{F}^{-1}\mathbf{Q}, \quad (25)$$

where \mathcal{F}^{-1} denotes inverse discrete Fourier transformation. However, such an explicit solution remains unsatisfactory for controlling the propagator to the fullest extent. Each of the time intervals τ_l has to be a positive real number, which is not guaranteed by inverse discrete Fourier transformation. Nevertheless, this issue can be addressed.

For discrete Fourier transformation, the necessary and sufficient condition to $\tau_l \in \mathbb{R}$ is $\forall m : Q_m = Q_{L-m}^*$. However, it is safe to assume that a realistic tight-binding lattice has a limit to the range of its nonzero hopping, i.e., $J_m \rightarrow 0$ for $m \gg M$. By using $L \gg 2M$, any given \vec{R}_m within $m \leq M$ can then be

realized with

$$\mathbf{Q} = [Q_0, \underbrace{Q_1, \dots, Q_M}_M, \underbrace{0, \dots, 0}_{L-2M-1}, \underbrace{Q_M^*, \dots, Q_1^*}_M]. \quad (26)$$

Then, $J_{L-m} \rightarrow 0$ for $m \leq M$ can guarantee that

$$\vec{R}_{L-m} \cdot (\hat{x} + i\hat{y}) = \frac{J_{L-m}}{\pi} Q_m^* \rightarrow 0. \quad (27)$$

As for positivity, note that the extra dimension Q_0 is conveniently not given by any \vec{R}_m since $m \neq 0$. By arbitrarily choosing an Q_0 that is large enough, we can then always guarantee $\tau_l > 0$. More simply, one can also calculate $\boldsymbol{\tau}$ with an arbitrary Q_0 and then ensure the complete positivity of $\boldsymbol{\tau}$ later by adding the same amount of sufficient time to each of its elements, which corresponds to an increase of Q_0 .

In Fig. 2, we demonstrate how to navigate \vec{R}_m up to $m = 3$ to an arbitrary position given destination using pulsed electric field. As shown in Figs. 2(b)–2(d), at the end of a sequence of pulsed electric field given by \mathbf{Q} , each \vec{R}_m of the lattice will reach its destination given by Eq. (23). Moreover, regardless of whether the identical pulses are of sufficiently small finite width or of ideal infinitesimal width, they will arrive at the same destination. For obvious geometry reasons, even if each \vec{R}_m had to change direction in an imperfect manner such as turning continuously, as long as the pulses are identical and they have the correct strength, the movement in each of the directions is affected evenly, which only equates the effect of changing Q_0 .

B. Floquet engineering

We then discuss turning a lattice into a simulator of a different lattice characterized by different hopping energies between n th nearest neighbors. Suppose we are to simulate a lattice with nonzero coupling up to M' th nearest neighbor, and we have a simulator lattice with up to M th nearest-neighbor coupling. As long as $M \geq M'$, by using a sequence of electric pulses, we will be able to navigate each \vec{R}_m of the simulator to undergo the same displacement as its counterpart \vec{R}'_m in the lattice it simulates during an arbitrary period of time T . Then,

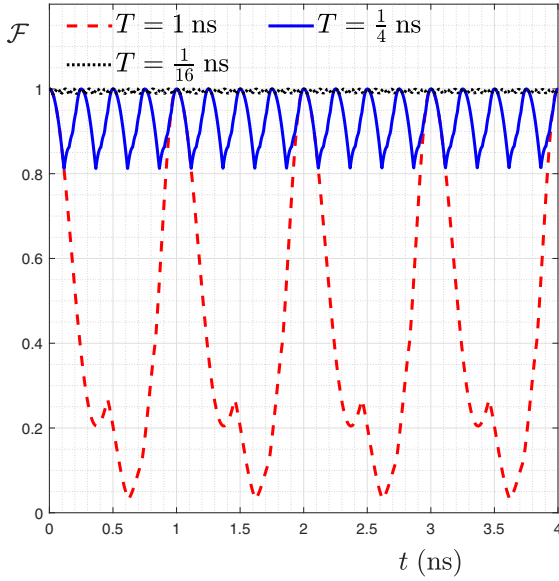


FIG. 3. Fidelity of quantum state evolution between the simulator and the lattice it simulates. The fidelity is given by Eq. (30), and the initial state is a single electron on an arbitrary single site with $j = 10$. The simulator lattice is characterized by Eq. (1) with $N = 20$ and $\mathbf{J} \equiv \{J_m\} = [3, 2, 1] \text{ ns}^{-1}$ up to the third-nearest-neighbor coupling. Under the navigation of $\mathcal{Q} = T \cdot [1, 0.2, 0.3, 0.6, 0.3, 0.2]$, it simulates the evolution of a lattice characterized by $\mathbf{J}' \equiv \{J'_m\} = [0.6, 0.6, 0.6] \text{ ns}^{-1}$. Pulses of electric field are characterized as with infinitesimal width.

the exact same procedure can be performed in continuous repetition, so \vec{R}_m would equal \vec{R}'_m at the end of each sequence.

For simplicity, we assume that the duration of each pulse sequence equals the time period of the evolution it simulates, i.e., $Q_0 = T$. (See Appendix C for otherwise). In this case, at each moment t that is the integer multiple of T , the propagator of the simulator will be equal to that of the lattice it simulates. In other words,

$$\forall l \in \mathbb{Z} : U(lT) = U'(lT), \quad (28)$$

in which $U(t) \equiv U(t, 0)$. Moreover, since each \vec{R}_m only moves at a fixed speed, there is a limit to how far $U(lT + \Delta\tau)$ can be away from $U'(lT + \Delta\tau)$ under $\Delta\tau < T$ if $\frac{1}{T} \rightarrow \infty$. More specifically, we have (see Appendix D)

$$\frac{1}{T} \gg \sqrt{\sum_m J_m^2} \Rightarrow U(t) \rightarrow U'(t), \quad (29)$$

which is estimated to be valid continuously for all time t .

As a simple numerical demonstration, we focus on the evolution of a particular initial state $|\psi(0)\rangle = c_j^\dagger |vac\rangle$ (see Appendix E for the justification) in a quantum ring, where the choice of j in c_j is irrelevant due to permutation symmetry. In Fig. 3, we compare the evolution of the simulator lattice $|\psi(t)\rangle$ and that of the lattice it simulates $|\psi'(t)\rangle$ with a simple fidelity given by

$$\mathcal{F} = |\langle \psi(t) | \psi'(t) \rangle|^2. \quad (30)$$

As can be seen from the figure, for all kicking frequencies, the fidelity returns to unitary periodically. During each

period, for the simulator with the lowest kicking frequency, the fidelity would drop to very low level before returning to unity. On the other hand, for the simulators with higher frequency, their fidelity remains close to unity throughout the whole period. There simply is not enough time for them to get very far. As the frequency of the kicking increases, the deviation of the simulator lattice from the lattice it simulates throughout the evolution would approach zero, which is consistent with the prediction of Eq. (29). In a special case, we also note that one can also recover dynamical localization if each of the simulated coupling coefficients is chosen to be zero.

IV. ROBUSTNESS

As far as the quantum state at moments where time t is an integer multiple of T is concerned, the effective Hamiltonian in our approach is entirely independent of the choice of pulse frequency, but the frequency does make a difference in the presence of additional influences. In the following, we will show that, in the limit of high kicking frequency, the response of the simulator to arbitrary additional influences will approach the same response as the lattice it simulates when subject to the same influences. Importantly, these additional influences can also include the effects of interacting with an environment.

Open quantum systems are usually studied under Markovian or non-Markovian master equations given by a series of conditions and approximations. Here, to introduce the environment, we instead employ the original untreated formalism [50,51], which reads

$$\mathcal{H} = \underbrace{H(t) \otimes I_E + I_S \otimes H_E}_{A(t)} + \underbrace{H_d(t) \otimes I_E + H_I}_{B(t)}, \quad (31)$$

where H_E generally denotes the Hamiltonian of the environment and I_S, I_E are identity operators on the lattice and the environment, respectively. $H_d(t)$ denotes defects introduced to the ideal lattice characterized by Hamiltonian $H(t)$. The full Hamiltonian is then separated into two parts: $A(t)$ includes only the undisturbed dynamics of the lattice and the independent evolution of the environment, while $B(t)$ characterizes additional influences from both within the lattice and the environment.

Given Eq. (31), we consider the rotating frame with respect to $A(t)$, which is characterized by a propagator

$$U_A(t) \equiv \mathcal{T} \exp \left[-i \int_0^t A(\tau) d\tau \right] = U(t) \otimes e^{-iH_E t}, \quad (32)$$

where $\mathcal{T} \exp$ denotes the time-ordered exponential. The evolution of the full quantum state $\psi(t)$ is then given by

$$\frac{\partial}{\partial t} \tilde{\psi}(t) = -i\tilde{B}(t)\tilde{\psi}(t), \quad (33)$$

$$\tilde{\psi}(t) \equiv U_A^{-1}(t)\psi(t), \quad (34)$$

$$\tilde{B}(t) \equiv U_A^{-1}(t)B(t)U_A(t). \quad (35)$$

Suppose $A(t)$ is given for the simulator lattice, its counterpart for the lattice it simulates $H'(t)$ is thereby denoted as $A'(t) = H'(t) \otimes I_E + I_S \otimes H_E$. Likewise and correspondingly,

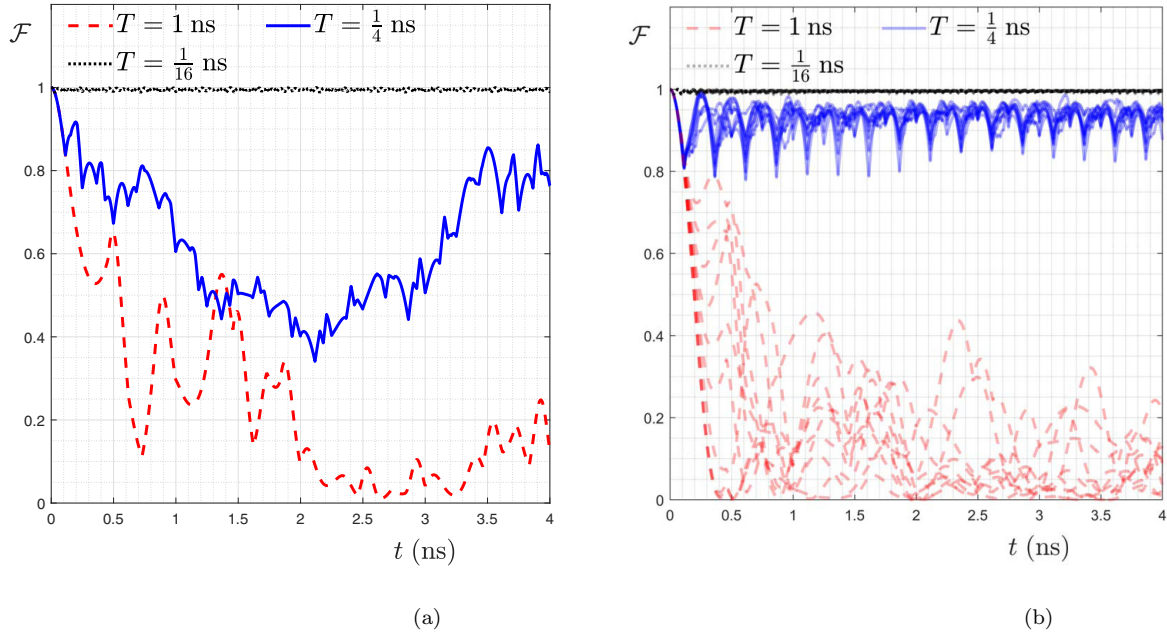


FIG. 4. Demonstration of lattice simulation under additional influence. The same parameters from Fig. 3 are employed, except for the following interventions: (a) An additional electric field characterized by $-aE = 2\sqrt{2}\pi\text{ns}^{-1}$ and Eq. (17); (b) Anderson noise characterized by Eq. (35) with randomized $\mathcal{A}_n \in [0, 10] \text{ns}^{-1}$, and for each different value of period T , 10 iterations are carried out and shown as superimposed semitransparent curves.

we can also denote $U'_A(t)$, $\tilde{\psi}'(t)$, $\tilde{B}'(t)$. However, the formalism of additional influences without rotating frame $B(t)$ must be the same for both the simulator and the system it simulates, i.e., $B(t) \equiv B'(t)$, which can be easily guaranteed for a wide range of additional influences, such as extra electric field, electron-electron interaction, or band-band interaction. We note that they are straightforward to show formally if the full system is transformed into a gauge where all the electric field is introduced as a scalar potential [e.g., Eq. (15)] instead of vector potential [e.g., Eq. (3)], which is allowed since the condition of Eq. (29), once established, would remain true under gauge transformation.

Apparently, even without additional influence, $A(t)$ would not approach $A'(t)$ regardless of the kicking frequency. However, when the kicking frequency is high, Eqs. (29) and (32) can give $U_A(t) \rightarrow U'_A(t)$, which is sufficient to ensure a robust simulation: For any given identical initial state $\tilde{\psi}(0) = \psi(0) = \psi'(0) = \tilde{\psi}'(0)$, Eqs. (33)–(35) would give $\tilde{B}(t) \rightarrow \tilde{B}'(t)$, then $\tilde{\psi}(t) \rightarrow \tilde{\psi}'(t)$ and eventually $\psi(t) \rightarrow \psi'(t)$. In other words, in the limit of high kicking frequency, the dynamics of the simulator would approach that of the lattice it simulates as long as they are subject to the same additional influence.

We note that, in the formalism above, the identical additional influences on the two systems are not required to be small. The difference between $\tilde{B}(t)$ and $\tilde{B}'(t)$ only grow linearly with the magnitude of $B(t)$, which can always be suppressed, in theory, with an increase of kicking frequency. Also, even in the case where a strong additional influence came to dominate the dynamics of both systems, since the additional influences on them are identical, one could still expect a high fidelity between their dynamics. Ideally, to an

observer unaware of the pulsed electric field, the simulator lattice could be indistinguishable from the lattice it simulates, which is not a general feature in Floquet engineering, where the effect of open quantum systems remains an open question [46,49,52]. Experimentally, however, since the single band model is itself an approximation [44], challenges remain in increasing kicking frequency, such as the effect of (interband) heating [53,54]. The simulation would be short-lived under high frequency kicking unless one could somehow suppress the heating from these arbitrarily shaped pulses.

For simplicity, the numerical demonstration is limited to intervention within the Hamiltonian, for which the same parameters from Fig. 3 are used. In Fig. 4(a), the evolution of the simulator lattice and the lattice it simulates are compared under the same additional static electric field. In Fig. 4(b), Anderson tight-binding model [4,55] is considered by introducing site-diagonal random potential [56] into the Hamiltonian in Eq. (1) as follows:

$$H(t) \rightarrow H_A(t) \equiv H(t) + \sum_n \mathcal{A}_n c_n^\dagger c_n, \quad (36)$$

where site-dependent \mathcal{A}_n characterizes randomized site energies that compromise translational invariance.

As can be seen from Fig. 4, when the sequence repeat frequency is low, the fidelity of the simulator will quickly diminish under either kind of additional influence as its evolution diverges from that of the system it simulates. However, as the frequency of the sequence increases, i.e., $\frac{1}{T} \rightarrow \infty$, the fidelity between the quantum evolutions of the simulator and that of the system it simulates approaches all-time unity. In other words, with a sufficiently high kicking frequency, one can ensure that the lattice responds to a wide range of addi-

tional influences in almost the exact same way as the system it simulates.

V. DISCUSSION AND CONCLUSION

In this paper, we developed an approach to control the evolution of single-band tight-binding quantum rings and lattices beyond nearest-neighbor coupling. By using a sequence of an identical pulsed electric field with strength given by Eq. (20) and intervals given by Eqs. (23) and (25), the propagator of a different lattice with up to the same hopping distance can be engineered within the well-defined space given by Eq. (12).

Moreover, by applying the sequence periodically at a high frequency, one tight-binding lattice with long-range hopping can simulate the evolution of a different lattice with a different array of hopping coefficients, as long as all the corresponding couplings are nonzero in the simulator. Provided that the hopping energies of the simulator are much greater than those in the system it simulates, the simulator can evolve at the same rate as the system it simulates. Otherwise, a time scaling would be required, but we note here that time scaling could also be useful as an equivalent of tuning the strength of environmental noise.

More importantly, if the frequency of the periodical sequence is high enough, we show that the evolution of the simulator lattice also responds similarly as the system it simulates to arbitrary additional influences. The most general formalism of external influences is employed, so the conclusion holds universally for all kinds of effects, such as additional electric field, Anderson noise, and environmental noises. It therefore stands to reason that, at a sufficiently high frequency, the simulator would ideally be indistinguishable from an actual lattice with the simulated parameters to an observer unaware of the pulses. However, we note that there are challenges yet to overcome experimentally, such as the effect of heating from the arbitrarily shaped electric pulses, especially if they were to be applied repeatedly at a high frequency.

As we have shown, the formalism and hence the approach in this paper can be directly generalized to lattices of higher dimensions. It can potentially help to realize a flexible simulation platform for arbitrary tight-binding single band lattices beyond nearest-neighbor coupling or even property manipulation of actual crystal lattices. In particular, since electric pulse sequences are easy to be altered instantaneously, the approach can be applied to studies on the quenching of lattice parameters. Furthermore, by considering electron-electron and band-band interaction as additional influences, applications to multiband and multielectron systems are also possible.

ACKNOWLEDGMENTS

This work is supported by National Natural Science Foundation of China (NSFC) under Grants No. 11775048 and No. 12047566, Fundamental Research Funds for the Central Universities (Grants No. N2005022, No. N2002005, No. 2412019FZ044, and No. 2412019FZ044), the LiaoNing Revitalization Talents Program (Grant No. XLYC1907033), and the Liaoning BaiQianWan Talents Program (Grant No. 201892126).

APPENDIX A: LACK OF PERIODICITY OF \mathcal{U}_1

In the following, we show that \mathcal{U}_1 cannot be periodical unless $N = 2, 3, 4, 6$. Since \mathcal{U}_1 satisfies Eq. (18), a necessary and sufficient condition to \mathcal{U}_1 being periodic thereby reads

$$\exists \vec{\alpha} \neq 0 : \mathcal{U}_1(\vec{\alpha}) = Ie^{-i\omega}, \quad (\text{A1})$$

where ω is an arbitrary phase factor. Note that the periodicity defined here is indifferent to the global phase. Consider realizing equal phase shifts for each Bloch momentum k under Eq. (13); it then follows that \mathcal{U}_1 is periodic if and only if

$$\exists \vec{\alpha} \neq 0 : \forall k, k' : [(\vec{r}_{1k} - \vec{r}_{1k'}) \cdot \vec{\alpha}] \in \mathbb{Z}. \quad (\text{A2})$$

We then focus on a regular N polygon with \vec{r}_{1k} as its vertices, e.g., the green regular hexagon in Fig. 1(a). For clarity, vertices are hereby denoted as capital letters such as A, B, C, D . Given any integer N , it is quite easy to show if \mathcal{U}_1 is not periodic:

$N = 3, 4$ notwithstanding, one can always find pairs of parallel diagonals(edges) AB, CD that satisfies $\vec{AB} = q\vec{CD}$, where q is the ratio of length between the pair of diagonals(edge).

Periodicity thereby demands that there exist a non-zero $\vec{\alpha}$ with which $\vec{AB} \cdot \vec{\alpha}$ and $\vec{CD} \cdot \vec{\alpha}$ are both integers for all possible pairs of AB, CD . However, if $\vec{AB} \cdot \vec{\alpha} = q\vec{CD} \cdot \vec{\alpha} \neq 0$ and q is irrational, the two inner products $\vec{AB} \cdot \vec{\alpha}$ and $\vec{CD} \cdot \vec{\alpha}$ cannot both be integers. And in the special case of $\vec{AB} \cdot \vec{\alpha} = 0$, the rotational symmetry guarantees that we can always find a different pair of diagonals (edge) $A'B', C'D'$ from a different angle to satisfy $\vec{A'B'} \cdot \vec{\alpha} = q\vec{C'D'} \cdot \vec{\alpha} \neq 0$.

Therefore, with a given N , \mathcal{U}_1 cannot be strictly periodical as long as a regular N polygon contains any pair of parallel diagonals (edge) whose lengths are incommensurable.

Finally, the length of the second shortest diagonal that is parallel to an edge of length d_0 is given by $d_2 = (1 + 2 \cos \frac{2\pi}{N})d_0$. Niven's theorem [57] states that, with $\sin \theta = x$, only if $x = 0, \pm \frac{1}{2}, \pm 1$, can both θ and x be a rational number. It then follows that d_0 and d_2 are incommensurable for $N = 5$ or any $N > 6$, which is therefore the sufficient condition to the nonperiodicity of \mathcal{U}_1 .

APPENDIX B: LACK OF PERIODICITY OF $U(t, \mathbf{0})$

In the following, we examine iteratively the necessary condition to propagator periodicity beyond nearest-neighbor coupling in the limit of $N \rightarrow \infty$.

Beginning with a lattice of up to an arbitrary M th nearest-neighbor coupling, its periodicity requires

$$\exists \mathbf{P}_M \neq 0, w \in \mathbb{R} : \Pi_{n=1}^M \mathcal{U}_n(\vec{R}_n) = Ie^{-i\omega}, \quad (\text{B1})$$

in which complex vector $\mathbf{P}_M \equiv \{P_n\}_{n=1, \dots, M}$, with $P_n = \vec{R}_n \cdot (\hat{x} + i\hat{y})$, characterizes each \vec{R}_n up to $n = M$. Similar to Eq. (A2), the proposition above entails an equal phase shift for each Bloch momentum k , which is straightforwardly characterized by

$$\forall k : \vec{r}_{Mk} \cdot \vec{R}_M = C_k - \sum_{n=1}^{M-1} \vec{r}_{nk} \cdot \vec{R}_n, \quad (\text{B2})$$

$$\forall k, k' : C_k - C_{k'} \in \mathbb{R}. \quad (\text{B3})$$

In the limit of $N \rightarrow \infty$, it is safe to consider every point of rational angle on the unit circle as a valid \vec{r}_{nk} and \vec{r}_{nk} as a continuous function of k . Equation (B3) thereby gives $\frac{\partial C_k}{\partial k} = 0$, i.e., $C_k \equiv C$.

$P_{M-1} \neq 0$ is then guaranteed whether $\vec{R}_M = 0$ or not: If $\vec{R}_M = 0$, then $P_M \neq 0$ entails at least one nonzero \vec{R}_n for $n < M$; and if $\vec{R}_M \neq 0$, then the left-hand side of the equation being dependent on k would demand the same for the right-hand side.

We then consider an arbitrary pair of k, k' that satisfies $\frac{M}{N}(k - k') = \frac{1}{2}$, which gives not only $\vec{r}_{Mk} + \vec{r}_{Mk'} = 0$ but also $\vec{r}_{nk} + \vec{r}_{nk'} \neq 0$ for any integer $n < M$. It thereby follows that

$$(\vec{r}_{Mk} + \vec{r}_{Mk'}) \cdot \vec{R}_M = 2C - \sum_{n=1}^{M-1} (\vec{r}_{nk} + \vec{r}_{nk'}) \cdot \vec{R}_n = 0. \quad (\text{B4})$$

By denoting $s = \frac{1}{2}(k + k')$, $\vec{R}'_n \equiv |\vec{r}_{nk} + \vec{r}_{nk'}| \vec{R}_n$ and considering $\vec{r}_{nk} + \vec{r}_{nk'} = |\vec{r}_{nk} + \vec{r}_{nk'}| \vec{r}_{ns} \neq 0$, we have

$$\sum_{n=1}^{M-1} \vec{r}_{ns} \cdot \vec{R}'_n = 2C. \quad (\text{B5})$$

In other words,

$$\exists P_{M-1} \neq 0, w \in \mathbb{R} : \prod_{n=1}^{M-1} U_n(\vec{R}'_n) = I e^{-iw}. \quad (\text{B6})$$

It is thereby shown that Eq. (B1) is the sufficient condition to Eq. (B6) in the limit of $N \rightarrow \infty$, which eventually leads to \mathcal{U}_1 being periodical as a necessary condition to the whole propagator being periodical.

APPENDIX C: TIME SCALING

Here, we address the case where the simulator is unable to guarantee $Q_0 = T$.

We first explain the challenge in guaranteeing $Q_0 = T$. Suppose the lattice it simulates is given by time-independent $\frac{\partial}{\partial t} \vec{R}'_m$, during a small period of time T , we have

$$\frac{\partial}{\partial t} \vec{R}'_m T \cdot (\hat{x} + i\hat{y}) = \frac{J_m}{\pi} Q_m. \quad (\text{C1})$$

For the simulator, the time required to navigate to $Q \equiv \{Q_m\}$ is then given by Q_0 . If a simulator lattice were to match the evolution of the lattice it simulates in real time, $Q_0 = T$ is a necessary requirement, but recall that there is a limit to its value: time intervals between pulses can only be a positive real number, i.e., $\tau_l > 0$, which is easier to ensure if the couplings in the simulator lattice are much greater than those in the lattice it simulates. Stronger coupling is therefore preferred in a simulator lattice. Otherwise, $Q_0 > T$ may be required, which necessitates a time scaling of the simulation.

In the case of time scaling, Eqs. (28) and (29) must be replaced by $U(lQ_0) = U'(lT)$ and $U(t) \rightarrow U'(t')$, respectively, with $t = \frac{Q_0}{T} t'$, $l \in \mathbb{Z}$. Note that symbols with prime notation are the counterparts in the lattice being simulated. Moreover, in the presence of additional influence, Eq. (31) has to be replaced by

$$\mathcal{H} = H(t) \otimes I_E + B(t), \quad (\text{C2})$$

$$\mathcal{H}' = H'(t') \otimes I_E + B'(t'), \quad (\text{C3})$$

$$B'(t') = \frac{Q_0}{T} B(t), \quad (\text{C4})$$

$$B(t) \equiv I_S \otimes H_E + H_d(t) \otimes I_E + H_I, \quad (\text{C5})$$

$$B'(t) \equiv I_S \otimes H'_E + H'_d(t) \otimes I_E + H'_I. \quad (\text{C6})$$

Apparently, the additional influence on the lattice it simulates is no longer identical, but scaled. Also, $H_E \neq H'_E$, so they can no longer be a part of $A(t), A'(t)$. Nevertheless, in the limit of high kicking frequency, by using $U_A(t) = U(t) \otimes I_E$ and $U'_A(t) = U'(t) \otimes I_E$, one can still show that

$$\tilde{B}'(t') \rightarrow \frac{Q_0}{T} \tilde{B}(t). \quad (\text{C7})$$

In other words, the amplitude of the effective additional influence is tunable, which could be useful.

APPENDIX D: STANDARD OF HIGH FREQUENCY

Here, we estimate the sequence frequency condition for all-time high fidelity of lattice simulation. We employ the same definition of fidelity given in Eq. (30) as well as the same initial state $c_j^\dagger |\text{vac}\rangle$ chosen in Appendix E. Also considering Eq. (18), the fidelity between $U(t)$ and $U'(t)$ is then given by

$$\begin{aligned} \langle \psi | \psi' \rangle &= \langle \text{vac} | c_j U^\dagger U' c_j^\dagger | \text{vac} \rangle \\ &= \langle \text{vac} | c_j \left\{ \prod_m \mathcal{U}_m(\Delta \vec{R}_m) \right\} c_j^\dagger | \text{vac} \rangle, \end{aligned} \quad (\text{D1})$$

$$\Delta \vec{R}_m \equiv \vec{R}'_m(t) - \vec{R}_m(t), \quad (\text{D2})$$

where $\vec{R}_m(t)$ and $\vec{R}'_m(t)$ are from the simulator and the lattice it simulates, respectively. Equations (7) and (13) thereby give

$$\langle \psi | \psi' \rangle = \prod_m \left\{ \frac{1}{N} \sum_k e^{-i[2\pi \vec{r}_{mk} \cdot \Delta \vec{R}_m]} \right\}. \quad (\text{D3})$$

With $l \in \mathbb{Z}$, we have $\vec{R}_m(lT) = \vec{R}'_m(lT)$. Also considering that $\vec{R}_m(t)$ moves at a fixed speed $\frac{J_m}{\pi}$, it is therefore guaranteed that

$$|\Delta \vec{R}_m(t)| < \frac{J_m T}{\pi 2}, \quad (\text{D4})$$

Since T is assumed to be small, the Taylor expansions of exponentials are only kept to their second order. Also considering $|\vec{r}_{mk} \cdot \Delta \vec{R}_m| < |\vec{r}_{mk}| \cdot |\Delta \vec{R}_m|$ and $\sum_k \vec{r}_{mk} = 0$, we have

$$\begin{aligned} \langle \psi | \psi' \rangle &\approx 1 - \frac{(2\pi)^2}{2N} \sum_{k,m} [\vec{r}_{mk} \cdot \Delta \vec{R}_m]^2 \\ &> 1 - \frac{1}{2} \sum_m |2\pi \Delta \vec{R}_m|^2, \end{aligned} \quad (\text{D5})$$

Recalling Eq. (D4), for $\langle \psi | \psi' \rangle \rightarrow 1$, we simply need

$$\sum_m |2\pi \Delta \vec{R}_m|^2 < \sum_m J_m^2 T^2 \ll 1, \quad (\text{D6})$$

which straightforwardly leads to the condition in Eq. (29).

APPENDIX E: CHOICE OF INITIAL STATE

To better reflect the behavior of the propagator, the choice of initial state in the numerical simulation involves the following considerations.

In the absence of electron-electron interaction, the multi-electron propagator has one-to-one correspondence with the propagator within the single-electron regime. And within the single-electron regime, we assume there is an initial wave function $|\psi_0\rangle$ that ensures $\{\epsilon_n(0)|\psi_0\rangle|n \in Z\}$ to be a complete basis of the single-electron Hilbert space. Equation (4) guarantees $[\epsilon_n(\phi), U(t)] = 0$ for arbitrary propagator

$U(t)$. Therefore, $U(t)|\psi_0\rangle = U'(t)|\psi_0\rangle$ is then sufficient to guarantee

$$\forall n \in \mathbb{Z} : U(t)\epsilon_n(0)|\psi_0\rangle = U'(t)\epsilon_n(0)|\psi_0\rangle. \quad (E1)$$

The completeness of $\{\epsilon_n(0)|\psi_0\rangle|n \in Z\}$ would then give $U(t) = U'(t)$. In other words, starting from $|\psi_0\rangle$, the lattice cannot evolve into the same quantum state unless the propagators are identical.

A particularly convenient $|\psi_0\rangle$ that ensures the completeness of $\{\epsilon_n(0)|\psi_0\rangle|n \in Z\}$ is simply the wave function of an electron perfectly localized to an arbitrary single lattice site.

-
- [1] S. Yang, Z. Song, and C. P. Sun, Wave-packet transmission of Bloch electrons manipulated by magnetic field, *Phys. Rev. A* **73**, 022317 (2006).
- [2] W. H. Hu and Z. Song, Dynamics of a tight-binding ring threaded by time-periodic magnetic flux, *Phys. Rev. A* **84**, 052310 (2011).
- [3] W. H. Hu, L. Jin, and Z. Song, Dynamics of one-dimensional tight-binding models with arbitrary time-dependent external homogeneous fields, *Quantum Inf. Process.* **12**, 3569 (2013).
- [4] E. B. Rozenbaum and V. Galitski, Dynamical localization of coupled relativistic kicked rotors, *Phys. Rev. B* **95**, 064303 (2017).
- [5] A. Marino, G. Torre, and R. Citro, Dynamical localization of interacting ultracold atomic kicked rotors, *Europhys. Lett.* **127**, 50008 (2019).
- [6] M. Fava, R. Fazio, and A. Russomanno, Many-body dynamical localization in the kicked Bose-Hubbard chain, *Phys. Rev. B* **101**, 064302 (2020).
- [7] V. Ravindranath and M. S. Santhanam, Dynamical transitions in aperiodically kicked tight-binding models, *Phys. Rev. B* **103**, 134303 (2021).
- [8] S. Longhi, Bloch oscillations in non-Hermitian lattices with trajectories in the complex plane, *Phys. Rev. A* **92**, 042116 (2015).
- [9] Y.-L. Xu, W. S. Fegadolli, L. Gan, M.-H. Lu, X.-P. Liu, Z.-Y. Li, A. Scherer, and Y.-F. Chen, Experimental realization of Bloch oscillations in a parity-time synthetic silicon photonic lattice, *Nat. Commun.* **7**, 11319 (2016).
- [10] S. C. Furuya, K. Takasan, and M. Sato, Control of superexchange interactions with DC electric fields, *Phys. Rev. Research* **3**, 033066 (2021).
- [11] D. H. Dunlap and V. M. Kenkre, Dynamic localization of a charged particle moving under the influence of an electric field, *Phys. Rev. B* **34**, 3625 (1986).
- [12] M. M. Dignam and C. M. de Sterke, Conditions for Dynamic Localization in Generalized AC Electric Fields, *Phys. Rev. Lett.* **88**, 046806 (2002).
- [13] S. Longhi, M. Marangoni, M. Lobino, R. Ramponi, P. Laporta, E. Cianci, and V. Foglietti, Observation of Dynamic Localization in Periodically Curved Waveguide Arrays, *Phys. Rev. Lett.* **96**, 243901 (2006).
- [14] S. Longhi, Dynamic localization and transport in complex crystals, *Phys. Rev. B* **80**, 235102 (2009).
- [15] A. Eckardt, M. Holthaus, H. Lignier, A. Zenesini, D. Ciampini, O. Morsch, and E. Arimondo, Exploring dynamic localization with a Bose-Einstein condensate, *Phys. Rev. A* **79**, 013611 (2009).
- [16] S. Longhi, Many-body dynamic localization of strongly correlated electrons in ac-driven Hubbard lattices, *J. Phys. Condens. Matter* **24**, 435601 (2012).
- [17] T. Nag, D. Sen, and A. Dutta, Maximum group velocity in a one-dimensional model with a sinusoidally varying staggered potential, *Phys. Rev. A* **91**, 063607 (2015).
- [18] E. M. Graefe, H. J. Korsch, and A. Rush, Quasiclassical analysis of Bloch oscillations in non-Hermitian tight-binding lattices, *New J. Phys.* **18**, 075009 (2016).
- [19] L. L. Li, D. Moldovan, P. Vasilopoulos, and F. M. Peeters, Aharonov-Bohm oscillations in phosphorene quantum rings, *Phys. Rev. B* **95**, 205426 (2017).
- [20] H. Kim, S. Park, R. Okuyama, K. Kyhm, M. Eto, R. A. Taylor, G. Nogues, L. S. Dang, M. Potemski, K. Je, J. Kim, J. Kyhm, and J. Song, Light controlled optical Aharonov-Bohm oscillations in a single quantum ring, *Nano Lett.* **18**, 6188 (2018).
- [21] H.-F. Cheung, Y. Gefen, E. K. Riedel, and W.-H. Shih, Persistent currents in small one-dimensional metal rings, *Phys. Rev. B* **37**, 6050 (1988).
- [22] L. P. Lévy, G. Dolan, J. Dunsmuir, and H. Bouchiat, Magnetization of Mesoscopic Copper Rings: Evidence for Persistent Currents, *Phys. Rev. Lett.* **64**, 2074 (1990).
- [23] D. Loss and T. Martin, Absence of spontaneous persistent current for interacting fermions in a one-dimensional mesoscopic ring, *Phys. Rev. B* **47**, 4619 (1993).
- [24] J. F. Weisz, R. Kishore, and F. V. Kusmartsev, Persistent current in isolated mesoscopic rings, *Phys. Rev. B* **49**, 8126 (1994).
- [25] S. Viefers, P. Koskinen, P. Singha Deo, and M. Manninen, Quantum rings for beginners: Energy spectra and persistent currents, *Phys. E Low-Dimensional Syst. Nanostructures* **21**, 1 (2004).
- [26] D. Boriskovsky and D. Cohen, Negative mobility, sliding, and delocalization for stochastic networks, *Phys. Rev. E* **101**, 062129 (2020).
- [27] J. Kohler, J. A. Gerber, E. Dowd, and D. M. Stamper-Kurn, Negative-Mass Instability of the Spin and Motion of an Atomic Gas Driven by Optical Cavity Backaction, *Phys. Rev. Lett.* **120**, 013601 (2018).
- [28] E. H. Cannon, F. V. Kusmartsev, K. N. Alekseev, and D. K. Campbell, Absolute Negative Conductivity and Spontaneous Current Generation in Semiconductor Superlattices with Hot Electrons, *Phys. Rev. Lett.* **85**, 1302 (2000).

- [29] X. L. Lei, N. J. M. Horing, and H. L. Cui, Theory of Negative Differential Conductivity in a Superlattice Miniband, *Phys. Rev. Lett.* **66**, 3277 (1991).
- [30] H. Krömer, Proposed negative-mass microwave amplifier, *Phys. Rev.* **109**, 1856 (1958).
- [31] G. C. Dousmanis, R. C. Duncan, J. J. Thomas, and R. C. Williams, Experimental Evidence for Carriers with Negative Mass, *Phys. Rev. Lett.* **1**, 404 (1958).
- [32] B. Nachtergaele, Y. Ogata, and R. Sims, Propagation of correlations in quantum lattice systems, *J. Stat. Phys.* **124**, 1 (2006).
- [33] M. Cheneau, P. Barmettler, D. Poletti, M. Endres, P. Schauß, T. Fukuhara, C. Gross, I. Bloch, C. Kollath, and S. Kuhr, Light-cone-like spreading of correlations in a quantum many-body system, *Nature (London)* **481**, 484 (2012).
- [34] X.-G. Zhao, G. A. Georgakis, and Q. Niu, Photon assisted transport in superlattices beyond the nearest-neighbor approximation, *Phys. Rev. B* **56**, 3976 (1997).
- [35] M. A. Jivulescu and E. Papp, On the dynamic localization conditions for dc-ac electric fields proceeding beyond the nearest-neighbour description, *J. Phys. Condens. Matter* **18**, 6853 (2006).
- [36] T. Mizoguchi and M. Udagawa, Flat-band engineering in tight-binding models: Beyond the nearest-neighbor hopping, *Phys. Rev. B* **99**, 235118 (2019).
- [37] Y. B. Gaididei, S. F. Mingaleev, P. L. Christiansen, and K. Ø. Rasmussen, Effects of nonlocal dispersive interactions on self-trapping excitations, *Phys. Rev. E* **55**, 6141 (1997).
- [38] G. Wang, J. P. Huang, and K. W. Yu, Nontrivial Bloch oscillations in waveguide arrays with second-order coupling, *Opt. Lett.* **35**, 1908 (2010).
- [39] P. G. Kevrekidis, The drastic role of beyond-nearest-neighbor interactions on discrete two-dimensional dynamical lattices: A case example, *J. Opt.* **15**, 044013 (2013).
- [40] J. Biddle and S. Das Sarma, Predicted Mobility Edges in One-Dimensional Incommensurate Optical Lattices: An Exactly Solvable Model of Anderson Localization, *Phys. Rev. Lett.* **104**, 070601 (2010).
- [41] T. Kohlert, S. Scherg, X. Li, H. P. Lüschen, S. Das Sarma, I. Bloch, and M. Aidelsburger, Observation of Many-Body Localization in a One-Dimensional System with a Single-Particle Mobility Edge, *Phys. Rev. Lett.* **122**, 170403 (2019).
- [42] X. Li and S. Das Sarma, Mobility edge and intermediate phase in one-dimensional incommensurate lattice potentials, *Phys. Rev. B* **101**, 064203 (2020).
- [43] J. Stockhofe and P. Schmelcher, Bloch dynamics in lattices with long-range hopping, *Phys. Rev. A* **91**, 023606 (2015).
- [44] D. Poletti and C. Kollath, Slow quench dynamics of periodically driven quantum gases, *Phys. Rev. A* **84**, 013615 (2011).
- [45] P. Delplace, Á. Gómez-León, and G. Platero, Merging of Dirac points and Floquet topological transitions in ac-driven graphene, *Phys. Rev. B* **88**, 245422 (2013).
- [46] C. M. Dai, Z. C. Shi, and X. X. Yi, Floquet theorem with open systems and its applications, *Phys. Rev. A* **93**, 032121 (2016).
- [47] S. H. Kooi, A. Quelle, W. Beugeling, and C. Morais Smith, Genesis of the Floquet Hofstadter butterfly, *Phys. Rev. B* **98**, 115124 (2018).
- [48] B. Pérez-González, M. Bello, G. Platero, and Á. Gómez-León, Simulation of 1D Topological Phases in Driven Quantum Dot Arrays, *Phys. Rev. Lett.* **123**, 126401 (2019).
- [49] A. Schnell, A. Eckardt, and S. Denisov, Is there a Floquet Lindbladian? *Phys. Rev. B* **101**, 100301(R) (2020).
- [50] C. Gardiner and P. Zoller, *Quantum Noise* (Springer-Verlag, Berlin, 2004).
- [51] H.-P. Breuer and F. Petruccione, *The Theory of Open Quantum Systems* (Oxford University Press, New York, 2007).
- [52] M. Hartmann, D. Poletti, M. Ivanchenko, S. Denisov, and P. Hänggi, Asymptotic Floquet states of open quantum systems: The role of interaction, *New J. Phys.* **19**, 083011 (2017).
- [53] A. Eckardt, Colloquium: Atomic quantum gases in periodically driven optical lattices, *Rev. Mod. Phys.* **89**, 011004 (2017).
- [54] G. Sun and A. Eckardt, Optimal frequency window for Floquet engineering in optical lattices, *Phys. Rev. Research* **2**, 013241 (2020).
- [55] P. W. Anderson, Absence of diffusion in certain random lattices, *Phys. Rev.* **109**, 1492 (1958).
- [56] J. T. Chalker, T. S. Pickles, and P. Shukla, Anderson localization in tight-binding models with flat bands, *Phys. Rev. B* **82**, 104209 (2010).
- [57] A. Korniłowicz and A. Naumowicz, Niven's theorem, *Formaliz. Math.* **24**, 301 (2016).